CHAPTER V

RESULTS AND DISSCUSION

This chapter will be divided into three main sections; namely kinetic study of Pt-Sn-K/γ-Al$_2$O$_3$ catalyst, hydrogen permeation study and membrane reactor study. Reaction rate constants and permeability coefficient obtained from the first two studies will be used in the development of mathematical models for packed bed and membrane reactors. Details of the studies are as follows.

5.1 Kinetic study

In the kinetic study section, the selection of three types of catalysts (Pt/γ-Al$_2$O$_3$, Pt-Sn/γ-Al$_2$O$_3$ and Pt-Sn-K/γ-Al$_2$O$_3$), the effect of internal and external mass transfer in catalyst pellets and the evaluation of rate constant of dehydrogenation of propane were considered.

5.1.1 Catalyst selection

A set of experiment was carried out to compare the performance of the Pt/γ-Al$_2$O$_3$, Pt-Sn/γ-Al$_2$O$_3$ and Pt-Sn-K/γ-Al$_2$O$_3$ catalysts for the dehydrogenation of propane to propylene. The reaction was operated at temperature of 773 K, GHSV of 12,700 hr^{-1} and the catalyst weight of 1x10^{-4} kg with 60 – 80 mesh size. The schematic diagram of the experimental setup is shown in Figure 4.1. The conversion and selectivity to propylene were measured as shown in Figure 5.1. The conversions of all the catalysts decrease with time on stream and after 1 hour they reach the asymptotes, at this point all the catalysts are highly selective to propene with selectivity as high as 95%.

The decrease of the conversion is due to the catalyst deactivation by coke formation. The results also show that the addition of Sn on the Pt/γ-Al_2O_3 catalyst improves the conversion of the Pt/γ-Al_2O_3 catalyst. This can be explained by the ensemble effect in which the addition of Sn results in an increase in Pt dispersion. As a result, the stability of the catalytic activity is improved from the reduced amount of coke depositing on the metal active sites (Barias et al.,1996; Krishnamuthy 1998). Moreover, the addition of Sn can improve the selectivity to propene due to blocking or poisoning of acid sites on the support (Barias et al.,1995). Figure 5.1 also shows that the Pt-Sn-K/γ-Al_2O_3 catalyst gave the highest conversion and the catalytic activity was stable at least within 5 hours of the study. This is because alkali metals such as potassium enhance hydrogen spillover on the catalyst surface and, thus, reduce the amount of coke depositing on the active site (Prasertdam et al.,1997) and that the alkali metals poisons the acid sites of the alumina support (Demiguel et al., 1995). In order to confirm that the amount of coke depositing on the metal active sites reduced with the addition of Sn and K. The CO adsorption technique was employed to measured the amount of metal active sites of fresh catalysts and the spent catalysts after 3 minute time on stream. The results are shown in Table 5.1. It can be calculated that after 3 minutes the fraction of metal active sites covered by coke on the Pt/γ-Al_2O_3, Pt-Sn/γ-Al_2O_3 and Pt-Sn-K/γ-Al_2O_3 catalysts are 91, 55 and 2%, respectively.

Table 5.1 Metal active site and propane conversion of fresh and spent catalyst

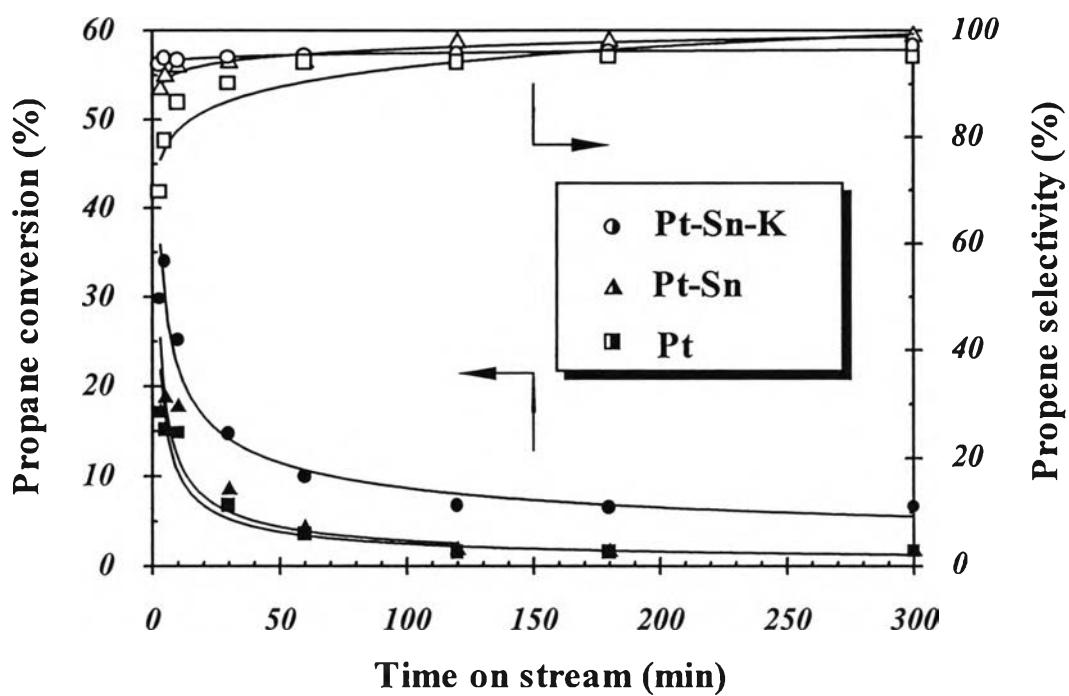| Catalyst	$N_{site}\times10^{-18}$			Conversion (%)	
	fresh	3 min	120 min	3 min	120 min
Pt-Sn-K	5.24	3.57	0.93	29.78	6.72
Pt-Sn	18.29	8.17	1.90	17.10	1.79
Pt	29.00	9.66	2.34	17	1.47

Figure 5.1 Conversion and selectivity of 3% propane on Pt/γ-Al₂O₃, Pt-Sn/γ-Al₂O₃ and Pt-Sn-K/γ-Al₂O₃ catalysts at 773 K, 0.1 MPa and GHSV of 12,700 hr⁻¹.

5.1.2 Effect of external and internal mass transfer

Before the determination of reaction rate constants, the operating conditions in which the effect of external mass transfer and internal mass transfer are negligible were determined both experimentally and theoretically. In this study only the Pt-Sn-K/Al_2O_3 catalyst was tested.

5.1.2.1 Effect of external mass transfer

The experiment was carried out using the same space velocity (GHSV) of 12,700 hr^{-1}, operating temperature of 773 K and catalyst mesh size of 60 – 80 mesh. The feed flow rate was varied between $2.5x10^{-7}$-$10.0x10^{-7}$ m^3(STP)/s. The results of propane conversion and time on stream were shown in Figure 5.2. There is no difference in propane conversion when the feed flow rate is higher than $7.5x10^{-7}$ m^3/s. This effect can also be checked theoretically by calculation as described in Appendix C. The results are shown in Table 5.2. It was found that the deviation of partial pressure of propane between the catalyst surface and the bulk gas are lower when feed molar flow rate increases, however, in all cases the deviation are less than 1%. It implies that in the range of experimental study the external mass transfer resistance should not play a significant role. However, the experimental results show that the effect can be negligible when the fed flow rate is higher than $7.5x10^{-7}$ m^3/s. This may be explained by the channeling effect of the catalyst bed. With small values of feed flow rate, only small amount of catalyst is used and, hence, the channeling effect will be more important. It should be note that the feed flow rate used in the kinetic study will be higher than $7.5x10^{-7}$ m^3/s to avoid this effect.

Table 5.2 Deviation of partial pressure of propane between catalyst surface and bulk gas

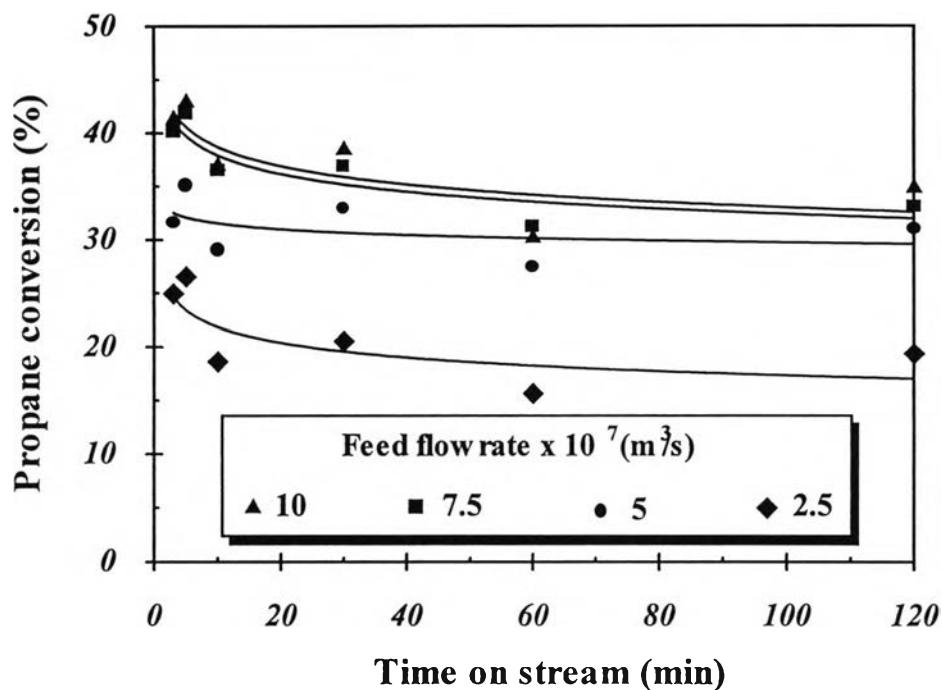| Feed molar flow rate x 10^7 (m^3/s)	Propane partial pressure different (%)
2.5	0.467
5.0	0.339
7.5	0.278
10.0	0.242

Figure 5.2 External mass transfer effect of 3% propane Pt-Sn-K/γ-Al₂O₃ catalysts at 773 K, 0.1 MPa and GHSV of 12,700 hr⁻¹.

5.1.2.2 Effect of internal mass transfer

Another set of experiment was carried out to investigate the effect of internal mass transfer. Three ranges of catalyst size of 60 – 80, 200 – 250 and 250 – 325 meshes were tested under the same operating condition, i.e. the amount of catalyst of 0.1 gram, operating condition of 773 K and space velocity (GHSV) of 12,700 hr⁻¹. The results of propane conversion and time on stream were shown in Figure 5.3. It was found that there is no difference between propane conversion within the range of catalyst size used in the study. The calculation results described in Appendix C were shown in Table 5.3, the effect of internal mass transfer can be ignored when a diffusional limitation term (Φ)<<1 (Froment, 1990). As a result, it can be concluded that there is no effect of internal mass transfer for the catalyst size smaller than 60 – 80 mesh.

Table 5.3 Diffusional limitation term (Φ) at different catalyst size

Catalyst size (mesh)	60/80	200/250	250/325
Φ	1.42×10^{-4}	1.35×10^{-5}	8.20×10^{-6}
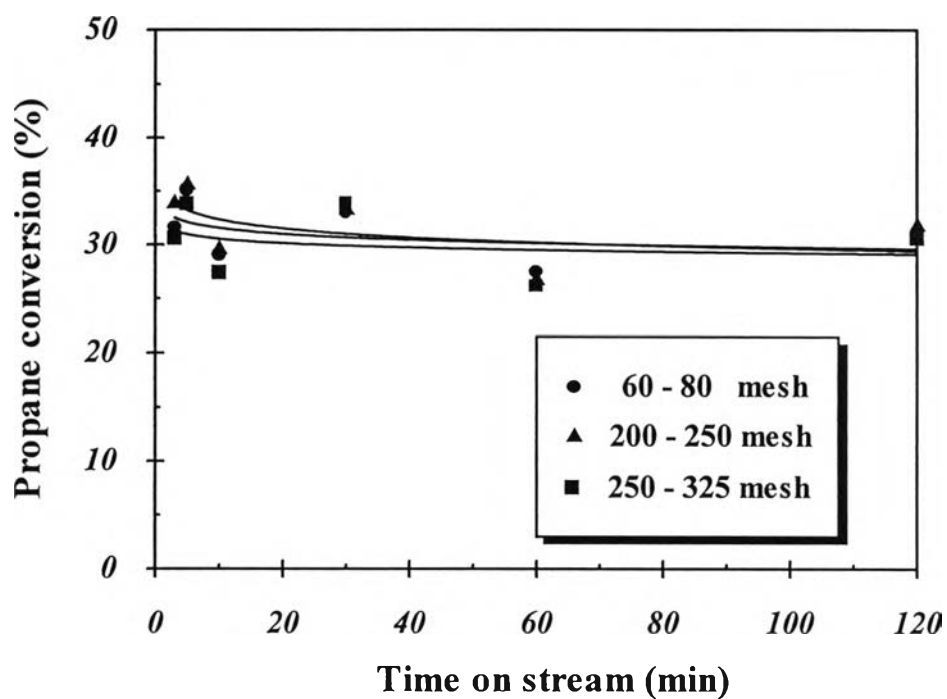
Figure 5.3 Internal mass transfer effect of 3% propane Pt-Sn-K/γ-Al$_2$O$_3$ catalysts at 773 K, 0.1 MPa and GHSV of 12,700 hr^{-1}.

5.1.3 Determination of the reaction rate constant

The dehydrogenation of propane to propene in this experiment was performed in a packed-bed microreactor. The rate expression for the dehydrogenation reaction can be expressed in the simple form of Eq.5.1 This form was also used to describe the dehydrogenation of ethane (Champagnie *et al.*,1992).

$$-r_A = k_{app} \left(p_A - \frac{p_B p_C}{K_{eq}} \right)$$

(5.1)

By assuming a plug flow reactor, the apparent rate constant k_{app} can be determined as (see Appendix D for further details).

$$k_{app} = \frac{F_{Ao}}{W_{cat}} \int_0^{X_A} \frac{dX}{\left(\frac{p_{Ao}(1-X)}{(1+y_{Ao}X)} - \frac{p_{A0}(\Theta_B + X)(\Theta_C + X)}{(1+y_{Ao}X)^2 K_{eq}} \right)}$$

(5.2)

In order to determine the reaction rate constants, it was assumed that the decrease of catalyst activity was due to the formation of coke on metal active sites and that the dehydrogenation of propane reached steady state within seconds (Larrson *et al.*, 1997 and 1998). Table 5.4 shows the apparent reaction rate constants, k_{app} calculated from Eq. 5.2 by using the conversions in Figure 5.1 for three catalysts at different time on stream. The apparent rate constant reflects the rate constant at the corresponding number of available active sites, N_{site} whose values are also shown in Table 5.1 Since the amount of coke depositing on the active sites varies with time on stream, it is better to show the rate constant based on the remained metal active sites of spent catalyst, N_{site} . The CO adsorption technique was employed to find the remained metal active site.

To compare the activity of the catalysts, the reaction rate constants based of the number of active sites, k_{site} is defined as follows.

$$k_{site} = k_{app}/N_{site}$$

(5.3)

Table 5.4 Metal active sites and reaction rate constant of $Pt/\gamma-Al_2O_3$, $Pt-Sn/\gamma-Al_2O_3$ and $Pt-Sn-K/\gamma-Al_2O_3$ catalysts at 773 K.

Catalyst	$k_{app}\times10^6$ [mol/(kg$_{cat}$·s·Pa)]		$k_{site}\times10^{28}$ [mol/(site·s·Pa)]		
	3 min	120 min	3 min	120 min	average
Pt-Sn-K	1.11	0.21	3.09	3.15	3.13
Pt-Sn	0.57	0.05	0.69	0.66	0.68
Pt	0.53	0.06	0.42	0.44	0.43
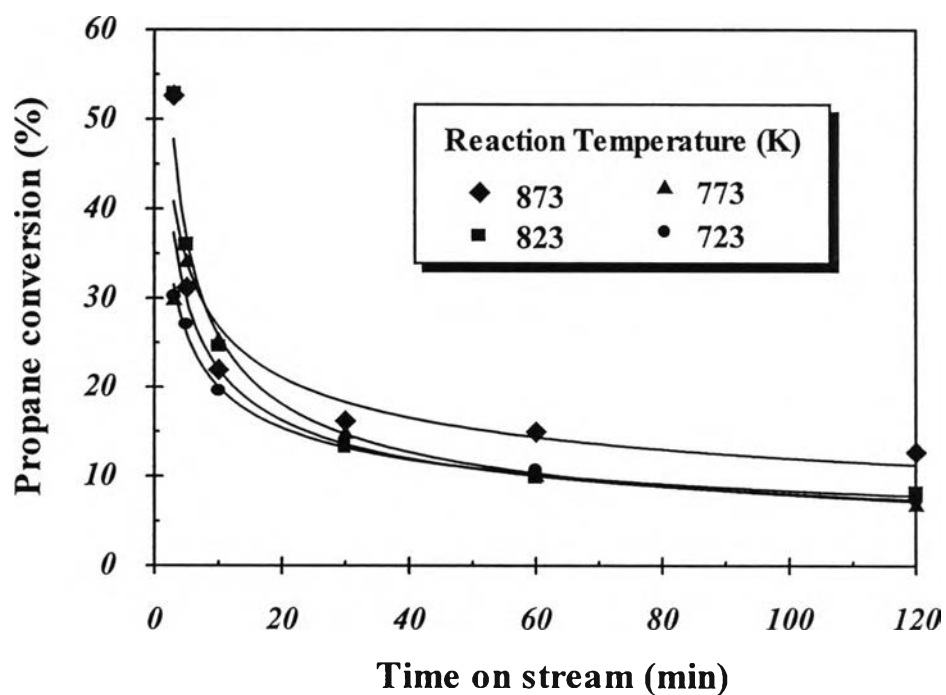
Figure 5.4 Conversion of 3% propane on $Pt-Sn-K/\gamma-Al_2O_3$ catalysts at difference reaction temperature.
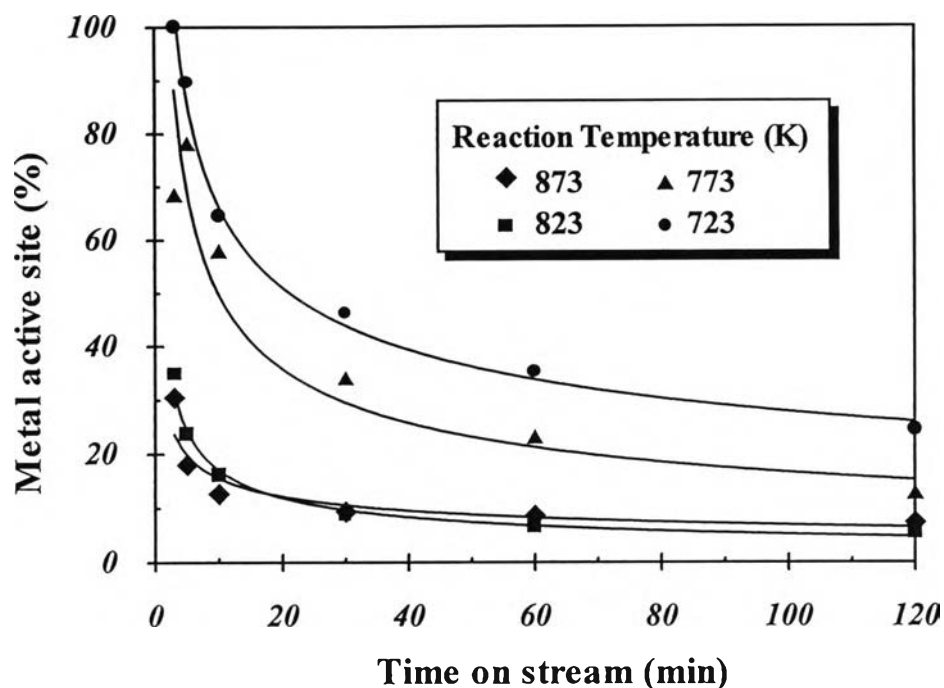
Figure 5.5 Remained metal active site (%) of Pt-Sn-K/γ-Al₂O₃ catalysts at difference reaction temperature.

The values of the reaction rate constants, k_{site}, are presented in Table 5.4 The reaction rate constant at 3 minute time on stream of the Pt-Sn-K/γ-Al₂O₃ (3.09x10⁻²⁸mol/site·s·Pa) is higher than that of the Pt-Sn/γ-Al₂O₃ (0.69x10⁻²⁸mol/site·s·Pa) and Pt/γ-Al₂O₃ (0.42x10⁻²⁸mol/site·s·Pa). In addition, the reaction rate constant for the Pt-Sn-K/γ-Al₂O₃ was confirmed using another experimental result with 20% propane. The value of 3.68x10⁻²⁸ mol/site·s·Pa was found to be close with the value from the 3% propane case. The obtained reaction rate constant confirms that the presence of potassium increases the strength of the metal active sites. From this result, the Pt-Sn-K/γ-Al₂O₃ catalyst was selected for use in membrane reactor studies.

To complete the determination of the rate constant of the Pt-Sn-K/γ-Al$_2$O$_3$ the reaction rate constants were determined at different temperatures ranging from 873 to 723 K.The results of conversion and metal active site with time on stream are shown in Figure 5.4 and Figure 5.5. It was found that conversion increases with the increase of temperature but the available metal active site decreases. This is because catalyst deactivation due to formation of coke on metal active sites was faster at higher temperature.

Table 5.5 Average reaction rate constant (k_{site}) at each reaction temperature

T(K)	Average (k_{site}) x 10^{28} [mol/(site$\cdot$s$\cdot$Pa)]
723	2.05
773	3.03
823	9.85
873	11.10

The apparent rate constants at different temperature are summarised in Table 5.5. The Arrhenius is plot carried out from the average k_{site} at all reaction temperatures shown in Figure 5.6 reveals the frequency factor of 6.14×10^{-24} mol/site$\cdot$s$\cdot$Pa and the activation energy of 62.7 kJ/mol. Arrhenius's equation can be determined as follow.

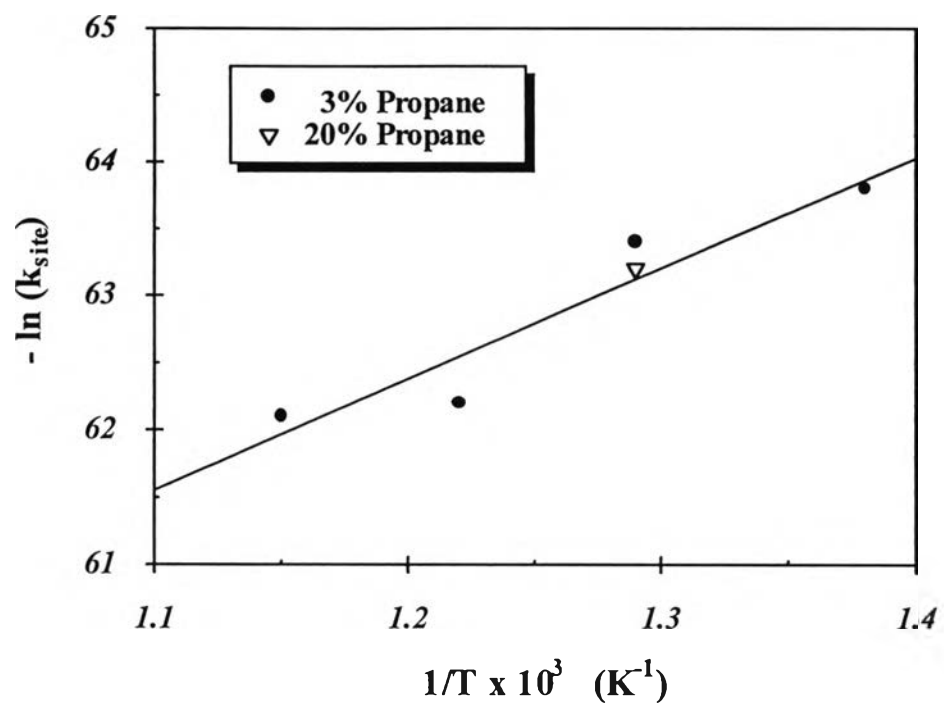$$k_{site} = 6.14 \times 10^{-24} \exp(-62,700/RT) \qquad (5.4)$$

Figure 5.6 Arrhenius plot of rate constant

5.2 Permeation study

Figure 4.3 shows the schematic diagram for the determination of hydrogen permeation rate. A set of experiment was carried out to investigate the permeability coefficient of hydrogen though the palladium membrane (α_H). The parameter α_H was obtained by fitting the experimental results with the model described in Appendix F.

Performing the material balance of hydrogen, a set of equations can be obtained

Tube side:

$$\frac{d\Phi_H^S}{dL} = -c\alpha_H \left(\sqrt{\beta_H^S} - \sqrt{\beta_H^T} \right)$$

(5.5)

Shell side:

$$\frac{d\Phi_H^T}{dL} = -\frac{d\Phi_H^S}{dL}$$

(5.6)

where α_H is the permeability coefficient of hydrogen though the palladium membrane.

The experiment was carried out under cocurrent mode. The hydrogen flow rate was fixed at approximately 2.55×10^{-5} mol/s while the nitrogen flow rate was varied between $3.93 \times 10^{-5} - 1.36 \times 10^{-4}$ mol/s. The amount of hydrogen permeating through the Pd membrane was measured at 573, 673, 773 and 873 K. It should be noted that the increase of nitrogen flow rate in the sweep side reduces the mass transfer resistance of the film in the sweep side.

The results are shown in Figure 5.7. The continuous lines are the average values of α_H. It was found that the film resistance at the membrane interface at the N_2 sweep side is not significant within the range of this study. The average values of α_H from each experiment are summarized in Table 5.6. It is obvious that the hydrogen permeation through the palladium membrane increases with the increase of operating temperature.

Table 5.6 Average H_2 permeability coefficient (α_H) at difference operating temperature

T(K)	$\alpha_{H,\ average}$ [mol/(s·m^2·Pa$^{0.5}$)]
573	2.55×10^{-7}
673	1.83×10^{-6}
773	8.88×10^{-6}
873	2.03×10^{-5}

Arrhenius's equation of the permeability coefficients of hydrogen though the palladium membrane can be determined by plotting the value $-\ln(\alpha_H)$ and $1/T$ as shown Figure 5.8. The frequency factor and the activation energy can be determined as 0.144 mol/(s·m^2·Pa$^{0.5}$) and 61.7 kJ/mol, respectively.

$$\alpha_H = 0.114\exp(-61{,}700/RT) \tag{5.7}$$
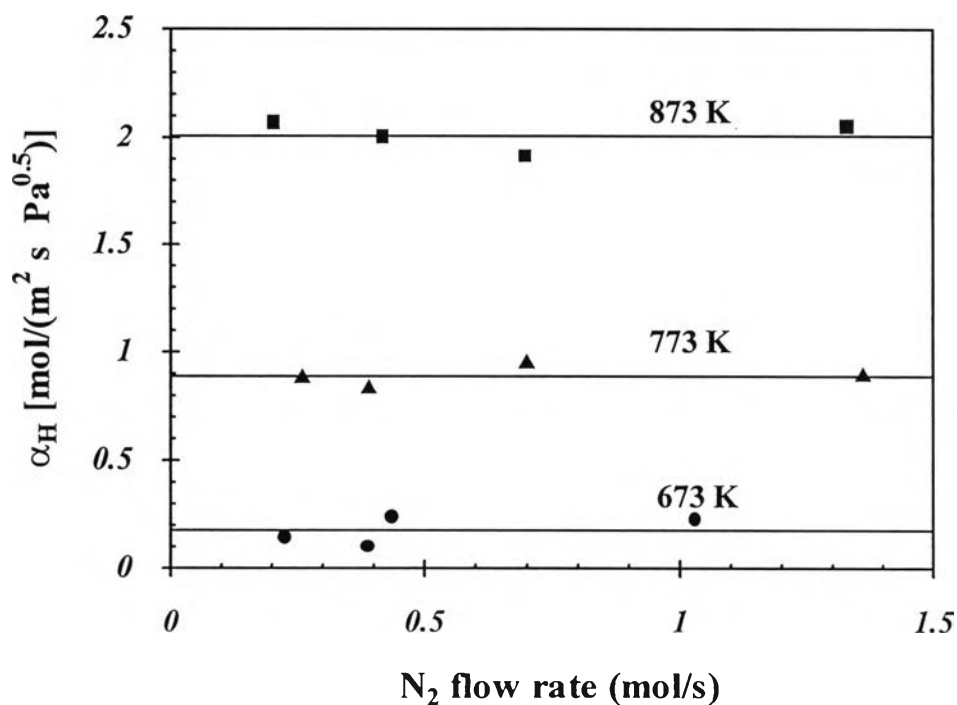
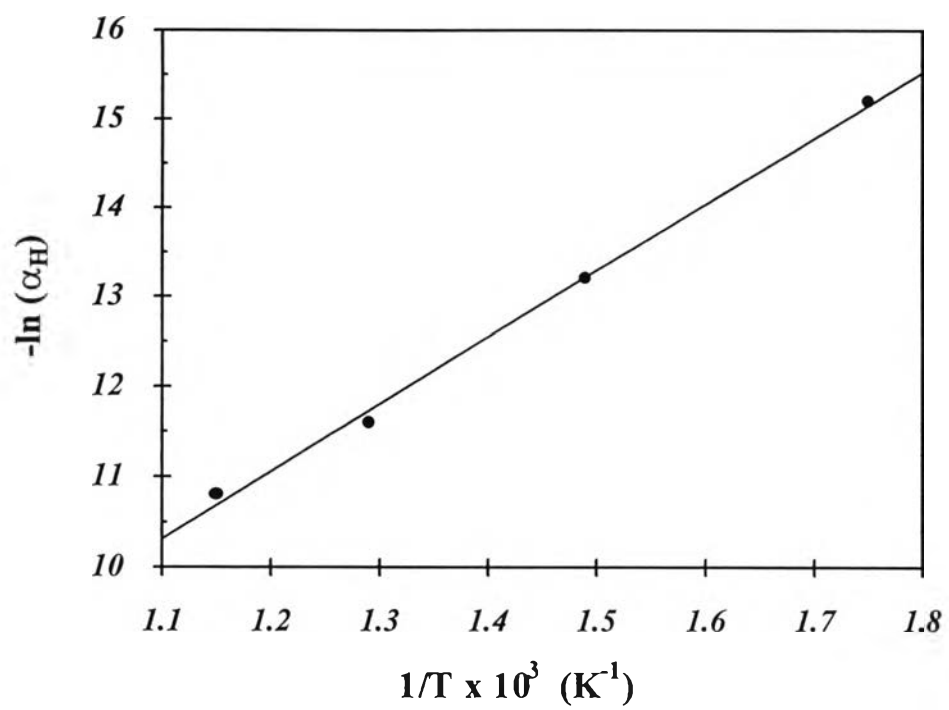**Figure 5.7** Permeability coefficient of H_2 through Pd membrane (α_H)

Figure 5.8 Arrhenius plot of H_2 permeability coefficient (α_H)

5.3 Membrane reactor study

5.3.1 Experimental study

The schematic diagram of membrane reactor used in this study is shown earlier in Figure 4.3. 16 grams of Pt-Sn-K/γ-Al$_2$O$_3$ were packed along the Pd membrane length. The experiments were carried out at atmospheric pressure on both sides of the membrane. The driving force of H$_2$ permeation through the membrane was created by using N$_2$ sweep gas flow in the tube side of reactor under cocurrent mode. The nitrogen flow rate was varied between $6.7 \times 10^{-5} - 4 \times 10^{-4}$ mol/s. In this study, feed propane of 3 and 20% balanced in N$_2$ was used as the reactant and fed to the reactor with GHSV of 90 h^{-1}. The composition of the retentate was analyzed by the gas chromatography.

Figure 5.9 shows the propane conversion as a function of the N$_2$ sweep gas flow rate and the corresponding equilibrium conversion. It wa found that within the range of experiment, the concept of the membrane reactor to selectively remove hydrogen from the reaction mixture does not show significant improvement effect as the propane conversion was only 3-5% higher than the equilibrium values. In addition, it was found that the conversion are slightly higher with the increase of nitrogen flow rate. This implies that the increase of partial pressure difference by reducing the partial pressure of hydrogen in the sweep side with nitrogen gas does not significantly affect the rate of hydrogen removal from the reaction side. It is suspected that the rather thick membrane with 100 μm thickness is the limiting factor for this system. To verify this hypothesis a mathematical modeling of the membrane reactor was carried out to simulate the performance of the membrane reactor under different operating condition as discussed in the next section.
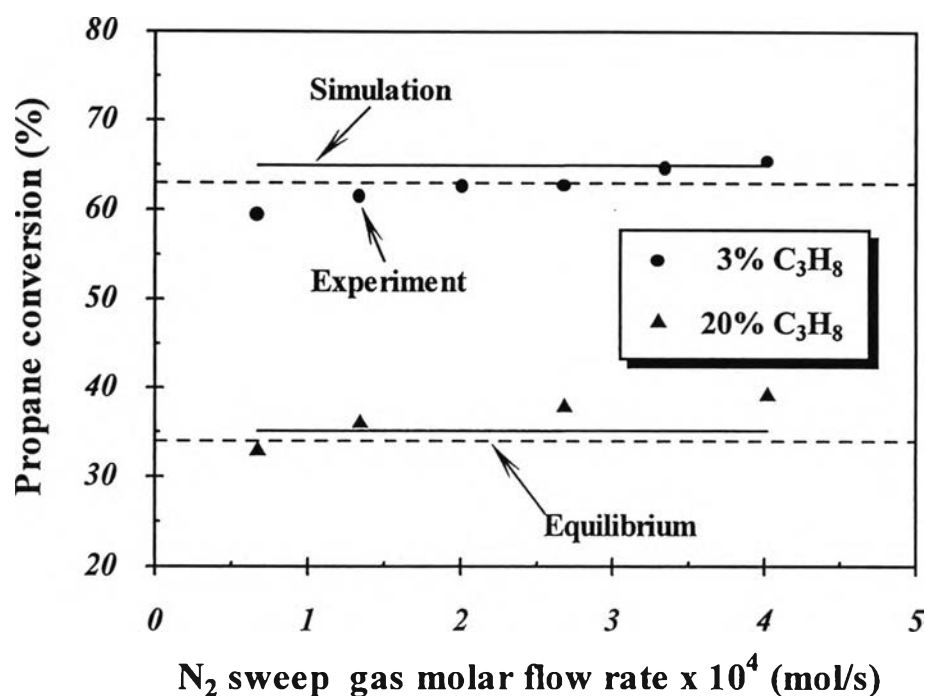
Figure 5.9 Effect of sweep gas molar flow rate on propane conversion at 773 K

5.3.2 Computer simulation

5.3.2.1 Mathematical modeling

    Psudo-homogeneous models for the case with and without radial effect were developed using the following assumption:

    – Steady-state operation

    – Isothermal

    – Co-current flow of sweep and feed gases

    Details of the development of models are given in Appendix G. For plug flug flow reactor, the 4th order Runk-Kutta was employed to integrate the differential equations while a finite difference method was used for the radial model. The followings summarize the sets of equations for both cases.

Plug flow model

Shell side:

$$\frac{d\Phi_i^S}{dL} = c_{S,1}\frac{v_i}{F_T^S}\left[\Phi_{C_3H_8} - \frac{\Phi_{C_3H_6}\Phi_{H_2}}{\left(\overline{F}_T^S K_{eq}/P^S\right)}\right] - c_{S,2}\alpha_i\left(\sqrt{\frac{\Phi_H^S P^S}{\overline{F}_T^S}} - \sqrt{\frac{\Phi_H^T P^T}{\overline{F}_T^T}}\right) \quad (5.8)$$

Tube side:

$$\frac{d\Phi_i^T}{dL} = c_{S,2}\alpha_H\left(\sqrt{\frac{\Phi_H^S P^S}{\overline{F}_T^S}} - \sqrt{\frac{\Phi_H^T P^T}{\overline{F}_T^T}}\right) \quad (5.9)$$

Radial diffusion model

Shell side

$$\frac{\partial\Phi_i^S}{\partial L} = b_{S,1}D_{im}^s P^S\left[\frac{1}{R^S - R_0^S}\frac{\partial}{\partial R}\left(\frac{\Phi_i^S}{\overline{F}_T^S}\right) + \frac{\partial^2}{\partial R^2}\left(\frac{\Phi_i^S}{\overline{F}_T^S}\right)\right] + \frac{b_{S,2}v_i P^S}{\overline{F}_T^S}\left[\Phi_{C_3H_8}^S - \frac{\Phi_{C_3H_6}^S\Phi_{H_2}^S}{K_{eq}\overline{F}_T^S/P^S}\right]$$

$$L = 0; \qquad \Phi_i^S = \Phi_{i,0}^S \quad (0 < R < 1)$$

$$R^S = 0; \qquad \frac{\partial}{\partial R}\left(\frac{\Phi_i^S}{\overline{F}_T^S}\right) = \frac{a_{S,1}\alpha_i}{D_{im}^S P^s}\left(\sqrt{\frac{\Phi_i^S\overline{P}_T^S}{\overline{F}_T^S}} - \sqrt{\frac{\Phi_i^T\overline{P}_T^T}{\overline{F}_T^T}}\right) \qquad (5.10)$$

$$R^S = 1; \qquad \frac{\partial}{\partial R}\left(\frac{\Phi_i^S}{\overline{F}_T^S}\right) = 0$$

Tube side:

$$\frac{\partial\Phi_i^T}{\partial L} = b_{T,1}D_{im}^T P^S\left[\frac{1}{R^T - R_0^T}\frac{\partial}{\partial R}\left(\frac{\Phi_i^T}{\overline{F}_T^T}\right) + \frac{\partial^2}{\partial R^2}\left(\frac{\Phi_i^T}{\overline{F}_T^T}\right)\right]$$

$$L = 0; \qquad \Phi_i^T = \Phi_{i,0}^T \quad (0 < R < 1)$$

$$R^T = 0; \qquad \frac{\partial}{\partial R}\left(\frac{\Phi_i^T}{\overline{F}_T^T}\right) = 0 \qquad (5.11)$$

$$R^T = 1; \qquad \frac{\partial}{\partial R}\left(\frac{\Phi_i^T}{\overline{F}_T^T}\right) = \frac{a_{T,1}\alpha_i}{D_{im}^T P^T}\left(\sqrt{\frac{\Phi_i^S\overline{P}_T^S}{\overline{F}_T^S}} - \sqrt{\frac{\Phi_i^T\overline{P}_T^T}{\overline{F}_T^T}}\right)$$

For the finite difference problems convergence was obtained by varying number of step size. In the radial diffusion model, the number of step sizes of the radial position of the tube and shell sides and the axial position of 10, 20 and 150,000, respectively, were used to obtain full convergence. In plug flow model, 5,000 step size in axial position was used.

Figure 5.9 compares the experimental and simulation results under the same operating condition. The predicted values from the simulation are comparable to the experimental values with error between 3 - 8 %. It is noted that the remained active sites used in this simulation were 6.3 %. This was obtained from the CO adsorption measurement of the spent catalysts. It was concluded that the model with the parameters obtained from the earlier study can be used to simulate the performance of the membrane reactor. This model will be used in the rest of the simulation with the additional assumption that the remained active site is constant at 6.3% regardless of the change off feed composition, sweep gas flow rate and temperature.

5.3.2.2 <u>Partial pressure profiles of reaction mixture and the effect of radial diffusion in Pd membrane reactor.</u>

Figure 5.10 and 5.11 shows average partial pressure profiles of reaction mixtures along the membrane length and H_2 partial pressure profile along radial position in reaction side at 773 K, respectively. In this study, a Pd selective layer with 10 μm thickness was selected in the simulation to obtain the high H_2 permeation rate. In figure 5.10, the basic concept of membrane is clarified as hydrogen is continuously removed from reaction zone along membrane length. Since the equilibrium composition can not be achieved due to the continuous removal of product hydrogen from the reaction side through the membrane. As a result, the forward reaction can continue.

To show the effect of radial dispersion, the radial hydrogen partial pressure profile at different dimensionless length were plotted as shown in Figure 5.11. It is found that on the reaction side the profiles are rather flat (less than 1-2 % difference), implying the negligible influence of dispersion effects in the membrane reaction. Dash lines in Figure 5.10 show the result from the plug flow model. It was found that the reaction mixture partial pressure does not differ significantly from the radial dispersion model except at the beginning of the reactor. At this position the hydrogen partial pressure gradient are the highest as shown in Figure 5.11. Thus in the Pd membrane under the range of this study, the permeability is not high enough to show significant radial dispersion effect.
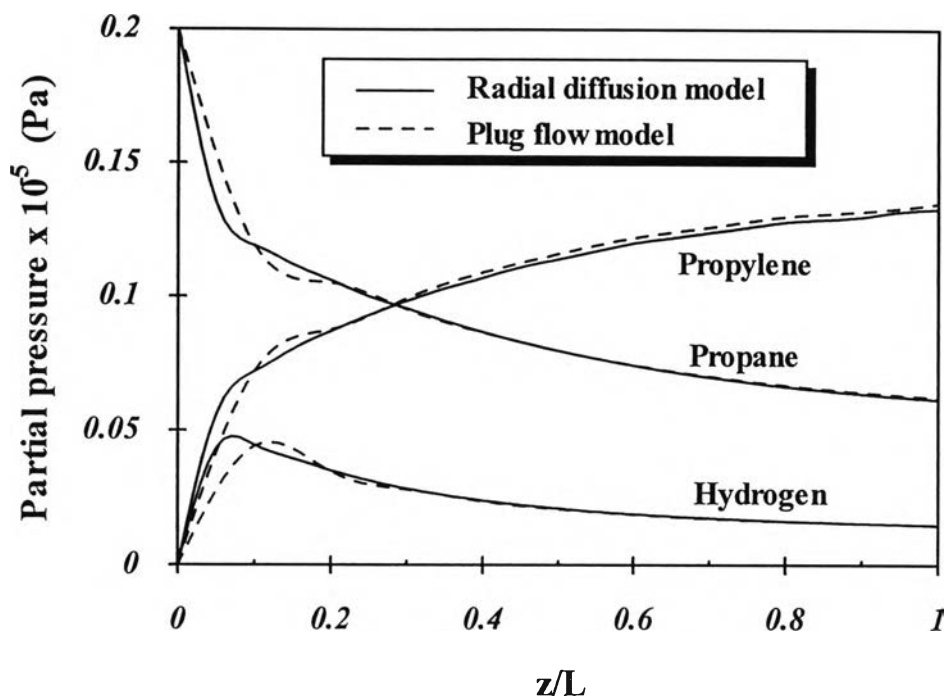
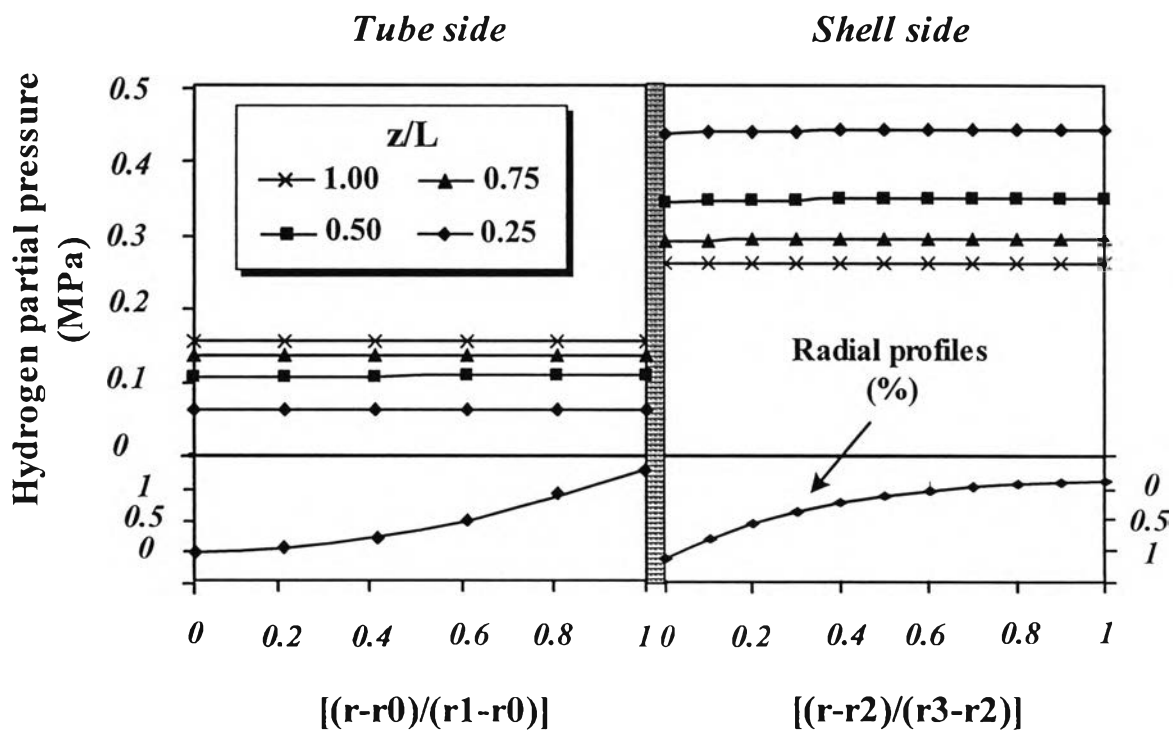**Figure 5.10** Partial pressure profiles of reaction mixture

Figure 5.11 H_2 partial pressure profile at radial position in reaction side at 773 K

5.3.2.3 Effect of membrane thickness on performance of membrane reactor

From the experimental result of the Pd layer with 100 μm thickness, the effect of sweep gas flow rates on membrane performance is not clear. Thus, this section will consider the effect of permeation rate by varying the thickness of the Pd layer. The results in Figure 5.12 shows that the membrane thickness significantly affects the propane conversion especially at high N_2 sweep gas flow rate. Therefore, it is obvious that the Pd layer with 100 μm thickness is not suitable for use because of the permeability is not high enough to obtain significant improvement.
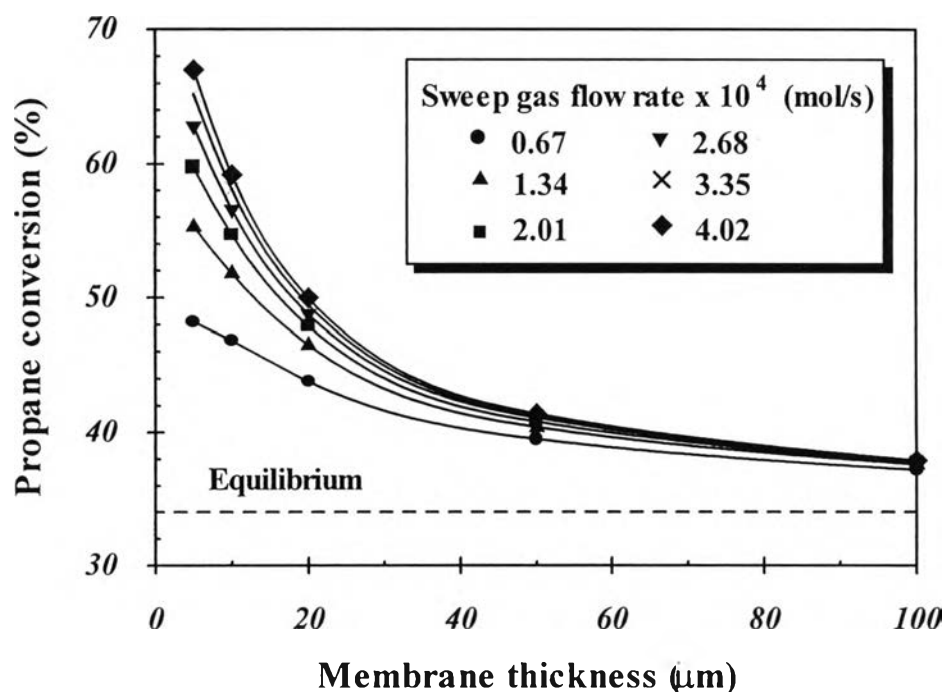

Figure 5.12 Conversion versus Pd layer thickness for difference N_2 sweep gas flow rate of 20% propane at 773 K and W/F of 13,200 kg$_{cat}$·s/mol.

5.3.2.4 Effect of W/F on membrane reactor performance

Figure 5.13 shows the effect of W/F for the feed propane with concentration of 3 and 20 % propane at 773 K. Feed molar flow rate was varied between $4x10^{-5}$-$4x10^{-3}$ mol/s and the catalyst weight was fixed at 16 g. From the results, for both of 3 and 20% propane in the membrane reactor, the conversion (solid line) was increased with W/F but in the conventional reactor the equilibrium conversion was the maximum attainable value.

At low W/F, the conversion difference between membrane reactor and conventional reactor was small and still below equilibrium values. When W/F increases, the rate of reaction was slow down and achieved the equilibrium conversion in the conventional reactor. However, for the membrane reactor, the conversion was not limited at the equilibrium conversion which was found in the conventional reactor due to the removal of H_2 from the reaction zone.
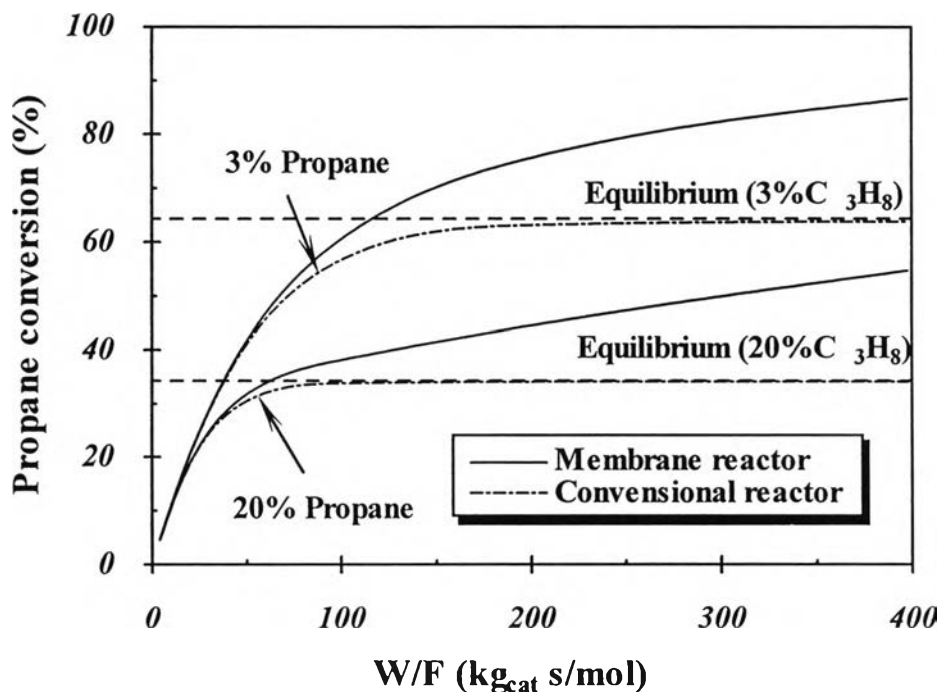

Figure 5.13 Conversion versus W/F of 3 and 20% propane at 773 K, sweep gas flow rate $2x10^{-4}$ mol/s.

5.3.2.5 Effect of temperature

Figure 5.14 shows conversion of 3 % propane at different operating conditions and the corresponding equilibrium conversion. It was found that at the same conversion the membrane reactor can be employed at lower operating temperature than the conventional system. The decrease of operating temperature does not only cause energy saving but the coke formation can also be reduced.
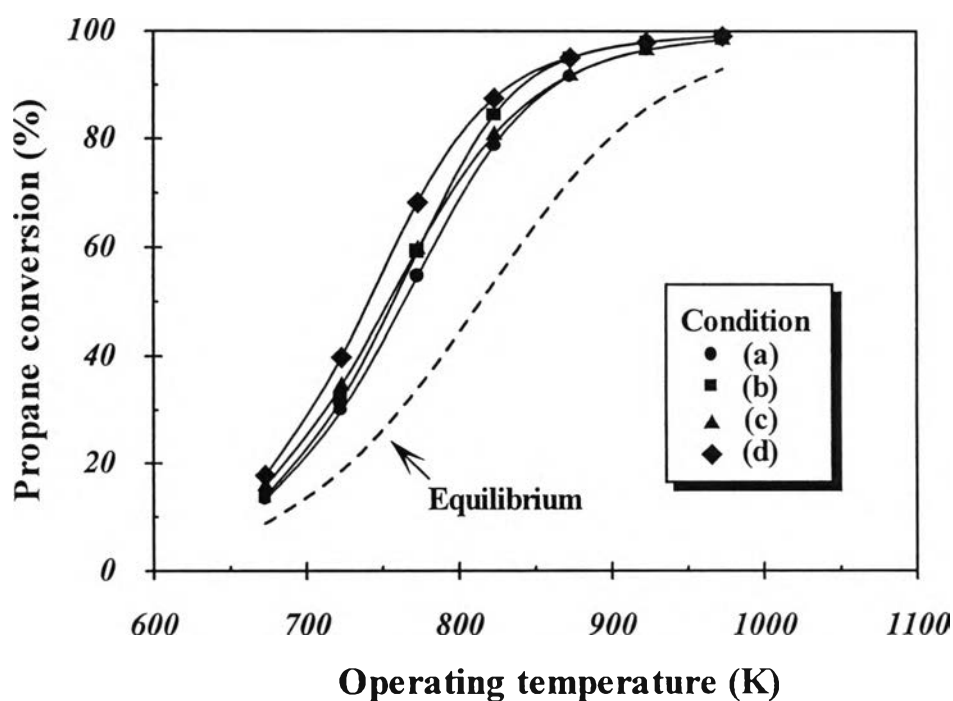

Figure 5.14 Conversion versus operating temperature of 3% propane at difference operating condition;

    a) W/F =13,200 kg_{cat}·s/mol, Pd thickness =10 μm, sweep gas flow rate = 2×10^{-4} mol/s;

    b) W/F =13,200 kg_{cat}·s/mol, Pd thickness =5 μm, sweep gas flow rate = 2×10^{-4} mol/s;

    c) W/F =13,200 kg_{cat}·s/mol, Pd thickness =10 μm, sweep gas flow rate = 4×10^{-4} mol/s;

    d) W/F =26,400 kg_{cat}·s/mol, Pd thickness =10 μm, sweep gas flow rate = 2×10^{-4} mol/s